communications earth & environment

ARTICLE

https://doi.org/10.1038/s43247-022-00540-4 OPEN

Limited Mediterranean sea-level drop during the Messinian salinity crisis inferred from the buried Nile canyon

Zohar Gvirtzman [1,2✉], Hanneke Heida[3], Daniel Garcia-Castellanos[3], Oded Bar[1], Elchanan Zucker[1,2] & Yehouda Enzel [2]

The extreme Mediterranean sea-level drop during the Messinian salinity crisis has been known for >50 years, but its amplitude and duration remain a challenge. Here we estimate its amplitude by restoring the topography of the Messinian Nile canyon and the vertical position of the Messinian coastline by unloading of post-Messinian sediment and accounting for flexural isostasy and compaction. We estimate the original depth of the geomorphological base level of the Nile River at ~600 m below present sea level, implying a drawdown 2–4 times smaller than previously estimated from the Nile canyon and suggesting that salt precipitated under 1–3 km deep waters. This conclusion is at odds with the nearly-desiccated basin model (>2 km drawdown) dominating the scientific literature for 50 years. Yet, a 600 m drawdown is ca. five times larger than eustatic fluctuations and its impact on the Mediterranean continental margins is incomparable to any glacial sea-level fall.

[1] The geological Survey of Israel, 32 Leibowitz St., Jerusalem 9692100, Israel. [2] The Fredy & Nadin Herrman Institue of Earth Sciences, The Hebrew University, Givat Ram, Jerusalem 9190401, Israel. [3] Gesciences Barcelona (GEO3BCN), Consejo Superior de Investigaciones Científicas (CSIC), Barcelona, Spain. ✉email: zohar@gsi.gov.il

5.96 million years ago (Late Messinian), when the connection between the Mediterranean Sea and the Atlantic Ocean was restricted, the entire Mediterranean became hypersaline, its marine fauna extinguished, and a kilometers-thick evaporite sequence was deposited on its floor[1,2] within a short period of ~640 ky[3,4]. This Messinian Salinity Crisis (MSC) is an exceptional event in Earth's history. The MSC sea-level fall is strongly debated for >50 years; with high-end estimates of >1500 m[1,5–8], intermediate estimates of 800–1500 m[9–15],or 630–900 m[16], and even minor estimates of 200–500 m[17,18]. These estimates are ingredients of the applied depositional models: from a nearly desiccated Mediterranean, with salt deposited in residual shallow hypersaline lakes[1,2,5], to a deep hypersaline-water body accumulating salt on its thousands-of-meters-deep floor[17–20].

A leading evidence for a large MSC sea-level drop is the upstream canyon incision of rivers (e.g., the Nile and Rhone), buried under thick sequences of sediment[2,6,21–25]. Elevation differences along (~2 km) and across (~1.5 km) the buried Nile canyon are considered as a measure for base-level drop[23] ignoring the possibility that at least a part of the canyon may have been subaqueous; moreover the thick Nile delta sediments also changed the vertical position of the buried canyon.

Here, we reconstruct the original elevation and shape of the Messinian Nile canyon, by correcting the buried Messinian erosion surface (MES[6]) for post-Messinian subsidence due to sedimentary loading (isostasy, lithosphere bending, and decompaction of underlying sediments). The results are the Messinian landscape immediately after its reflooding and before any Pliocene sedimentation (ignoring a few tens of m difference between the Early Pliocene and the present sea level[26]).

On the reconstructed landscape, we identify the geomorphologic base level of the MSC-Nile River, where the reconstructed river profile attains a subhorizontal slope. The paleo-shoreline should be along this relatively flat region, possibly where river profile steepens again (exact horizontal location within the subhorizontal region is of little relevance for restoration of vertical isostatic motions). With unloading the water above the base level, we restore the pre-flooding Messinian landscape, i.e, during maximal drawdown.

Finally, we show that our conclusion about limited drawdown is robust in spite of the uncertainties related to the restoration process, although we cannot exclude that the sea was temporarily at different levels during the drawdown.

Geological observations. Near the present-day coast, the Messinian Nile canyon is buried 3000 m under the flat delta plain (Fig. 1a). About 100 km to the south, Near the city of Cairo, the canyon base is ~1500 m below the surface and its shoulders nearly reach the surface[23]. Farther south, beyond the seismically-mapped plain, the canyon size and depth are uncertain. Approximately 1000 km south of Cairo, near Aswan, Early Pliocene brackish ostracods at the base of a 200 m deep canyon fill[27,28] raised the hypothesis that an Early Pliocene marine invasion of the canyon had reached Aswan, portraying the boundaries of the earlier MSC incision ~1200 km away from the present day coast[24,29]. However, fauna reexamination[30,31] showed a poor assemblage of rare and non-marine ostracods with a wide age range. This fauna could have been reworked from Cretaceous or Paleogene outcrops, as observed in many Pliocene sediments along the Nile Valley[31]; i.e., the near-Aswan canyon could have been subaerially excavated and buried before or after the MSC.

Examining stratigraphic data along the Nile Valley may clarify the uncertain inland extent of the MSC Nile canyon. Near Helwan, ~15 km south of Cairo, a water well reached the bottom of the canyon at 550 m[32,33] below sea level (mbsl) and a few km farther south another water well reached the bottom of the canyon at 200 mbsl[29]. This abrupt depth change from 1200 m to 200–550 along only 15 km, indicates a paleo-knickzone, separating a deep gorge from a much shallower upper valley. Moreover, this knickzone approximately coincides with an Early Pliocene sedimentologic transition in the canyon fill from deep-water claystone[34] to shallow marine and tidal limestones that continue ~150 km farther south until Beni-Suef[34–38]. Farther inland, Pliocene exposures consist of fluvial-lacustrine sediments[31,34,39,40]. These sedimentological data indicate that the early Pliocene marine invasion filled a deep gorge up to the Cairo-Helwan region, continuing ~150 km southward as a narrow and shallow marine embayment. From there, non-marine lacustrine environments extended farther inland.

Flexure produced by the Nile delta isostatic load. Most MSC flexural studies[14,41–45] are initiated with pre-MSC relief and forward model the vertical motions caused by deposition and erosion of pre-assumed masses of salt, water, and eroded material. Here we question the pre-assumed water mass and utilize a different approach; the present-day relief is the reference and we backward model (restore) the topography immediately after the MSC, by isostatically unloading sediments that accumulated since. Similar exercise[15], conducted for the Po Plain and the north Adriatic Sea, concluded that an 800-900 m drawdown best explains buried erosional features; and the same approach applied for the Western Mediterranean yielded 1100–1500 m drawdown[46]. The advantage in backward modeling is the well-known current relief and the unloaded sediments mass from seismic and well data. The source of uncertainty in the tectonic correction, which could be large[15] particularly in tectonically active areas. Sicily, the Apennines, Crete, and Cyprus have uplifted thousands of meters since the end of the Miocene; the Ionian, Herodotus, and northern Levant basins subsided hundreds or thousands of meters towards nearby subduction zones[47–49]. Fortunately, northern Egypt is far from any plate boundary with minimal tectonic activity. The continuous flow of River Nile along thousands of kilometers without significant post-Messinian incision, excludes the possibility of regional uplift. On the other hand, the lack of post-Messinian sedimentation outside of the Nile Valley indicates negligible regional subsidence. Moving offshore, the closest location of post-Messinian tectonic activity is observed 150–200 km north of the Messinian canyon along the Rosetta and Temsah Fault systems[50]. We estimate that this remote tectonic activity had minor influence on the restored canyon.

Taking advantage of the minor post-MSC tectonic activity in the Nile delta, we focus on the influence of the thick Nile delta load (2000 m and 3000 m contours, Fig. 1a) on the paleo-Nile canyon located > 100 km to the south. 2D-treatment of this problem[44,45] provides uplifted canyon shoulders, but still below sea level (Fig. 1b). However, we hypothesize that a 3D-calculation considering a ~4 km-thick off-plane load should yields much higher canyon shoulders (*e* Fig. 1b). Our analysis indicates that the shoulders of the Messinian Nile canyon were significantly higher than the "normal" sea level before and after drawdown (*e* in Fig. 1b); due to the delta-load induced flexure, this positive topography was lowered after the Messinian. Without correcting for this pre-flexure topography, the magnitude of the sea-level drop is overestimated (Fig. 1b).

Geological markers for the fallen sea level. Another reason for overestimating the magnitude of the MSC drawdown is ignoring the possibility that the downstream portion of the canyon may

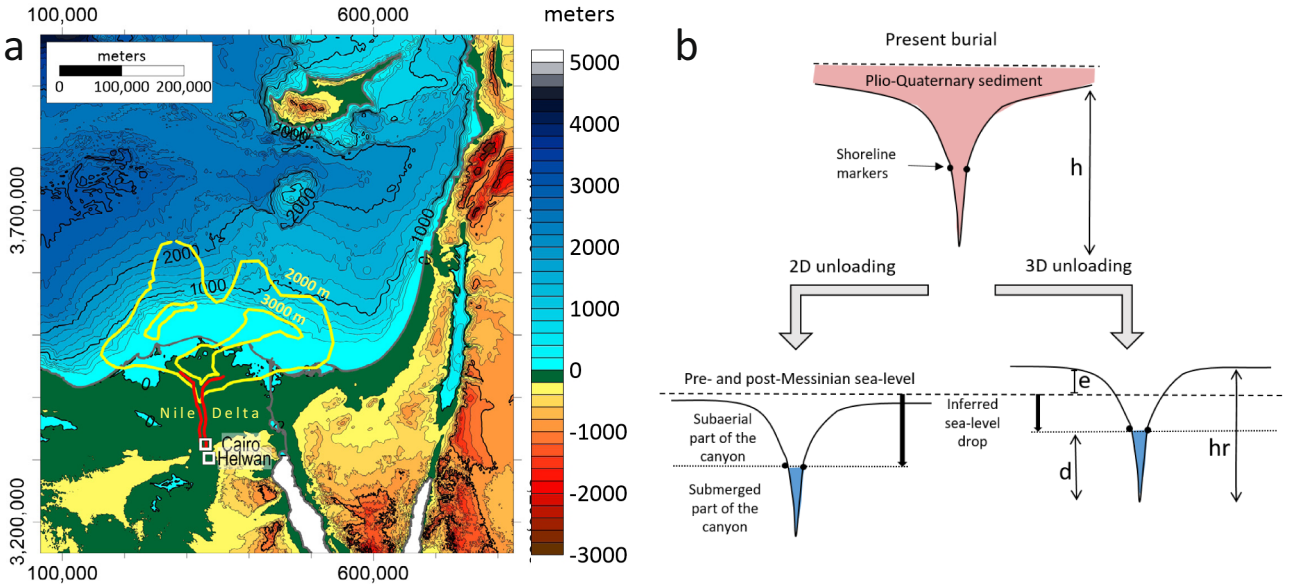

Fig. 1 The expected influence of the Nile delta load on the adjacent Messinian canyon. a Present-day topography and bathymetry. Red line outlines buried canyon walls[23]. Yellow lines are the 2000 and 3000 m[50] thickness contour of the Pliocene-Quaternary section showing that the main sedimentary load is located north of the canyon. **b** Schematic illustration of the difference between 2D and 3D restoration of the original vertical position of the Messinian canyon. Upper panel shows the present day buried canyon under Pliocene-Quaternary rocks. Left panel illustrates that in 2D analysis, canyon remains fully below present day sea level. Right panel illustrates that 3D analysis, considering the off plane load, is expected to provide higher canyon shoulders. h - the height difference between canyon thalweg and shoulders. hr - the same after sediment unloading (hr < h). e - elevation of canyon shoulders asl. d - water depth in the submerged part of the canyon. The inferred sea level drop is $\Delta_{sea\ level} = hr - e - d$.

have been, at least, partly submerged below the fallen sea level (*d* in Fig. 1b). The challenge is to recognize indicators of the fallen MSC sea-level, including 1) Changes in the slope of the river thalweg as indicators of land-sea transition[45]. 2) Sedimentary facies characterizing continental-to-marine or shelf-to-slope transitions[15,51,52]. 3) Buried scarps of shoreline terraces[10,11,13]. 4) Flat truncations indicating subaerial erosion[11]. 5) Geomorphic erosional surfaces/features distinguishing between subaerial and submarine channels[16].

Here we combine two observations constraining the amplitude of sea-level drop: a) the knickzone height generated by the upstream-migrating Nile incision, which constrains the minimal (partial) drawdown, excluding the downstream part of the valley. b) The transition from a sub-horizontal to a steeper river profile marking the transition from fluvial to submarine flow. Such a transition is observed in rivers continuously extending on-to-offshore as submarine canyons; e.g., the Gauping River-Canyon[53] (southwest Taiwan) and the LIobregat River-Foix Canyon[54] (Spain), with nearly horizontal thalweg approaching the coastline or shelf edge and much steeper thalweg offshore. Over geological time scales, near their base level and mouth, river profiles flatten. Therefore, the near-horizontal river profile and its slope break with the submarine canyon indicate the presence of a regional base level.

Results

Restoring the original topography. Restoring the original topography requires the Pliocene-Quaternary thickness (Fig. 2a), and involves calculating the subsidence due to compaction of pre-Pliocene sediments (Fig. 2b) and the flexural deflection due to the weight of the Pliocene-Quaternary sediment (Fig. 2c) and the evaporated water layer (Fig. 2d). Figure 2e, f present the observed and restored base Pliocene surface. Compaction maps calculated for various lithologies and deflection maps with varying elastic thickness and/or water layers are in Supplementary Fig. S1.

The restored landscape is a few hundred meters above the pre- and post-MSC sea level (Fig. 3b); its present depth below the flat delta plain expresses the post-Messinian subsidence due to flexural bending of the lithosphere and compaction of pre-Pliocene sediments (Fig. 2a, b). The canyon's longitudinal profile (Fig. 4a) illustrates that this upward restoration reached ~750 m near Cairo and ~2000 m at the base of the paleo-continental slope. Confirming our hypotheses, the restoration quantifies the elevated canyon shoulders (*e* in Fig. 1b) and the original canyon depth ($hr < h$ in Fig. 1b). For example, 60 km north of Cairo (Section 4, Fig. 4d), the restored shoulders are ~300 m above the pre- and post-MSC sea level, and the shoulder-to-thalweg relief drops from 1500 m in the buried surface to 1000 m in the restored landscape.

The longitudinal river profile further illustrates that the height of the Cairo-Helwan knickzone is reduced from 650 m in the buried profile to 400 m in the restored profile (Fig. 4a). Downstream, the profile flattens to near horizontal with ± 100 m elevation differences for the $20 < Te < 50$ km range of elastic thicknesses. This nearly horizontal segment extends ~40 km downstream to a slope break (knickpoint), where the concave profile abruptly steepens and becomes convex.

We interpret the Cairo-Helwan knickzone as the southernmost location of the Messinian retrogressive incision, separating the MSC canyon gorge from the pre-MSC upstream valley. This knickzone most probably was characterized by a series of high bedrock waterfalls[55] held by hard Mesozoic carbonates[23]), accommodating most of the sea-level drop. From the base of this inferred knickzone, the river slope gradually decreased towards the inferred base level (Fig. 4a). The concave-convex knickpoint is interpreted as the coastline, where the subaerial river flow was transformed into a submarine turbiditic flow that formed a subaqueous canyon.

The depth of the inferred MSC coastline is ~650 mbsl for all curves calculated with elastic thickness $20 < Te < 50$ km. Differences of 100–200 m between $Te = 20$ and $Te = 50$ km are

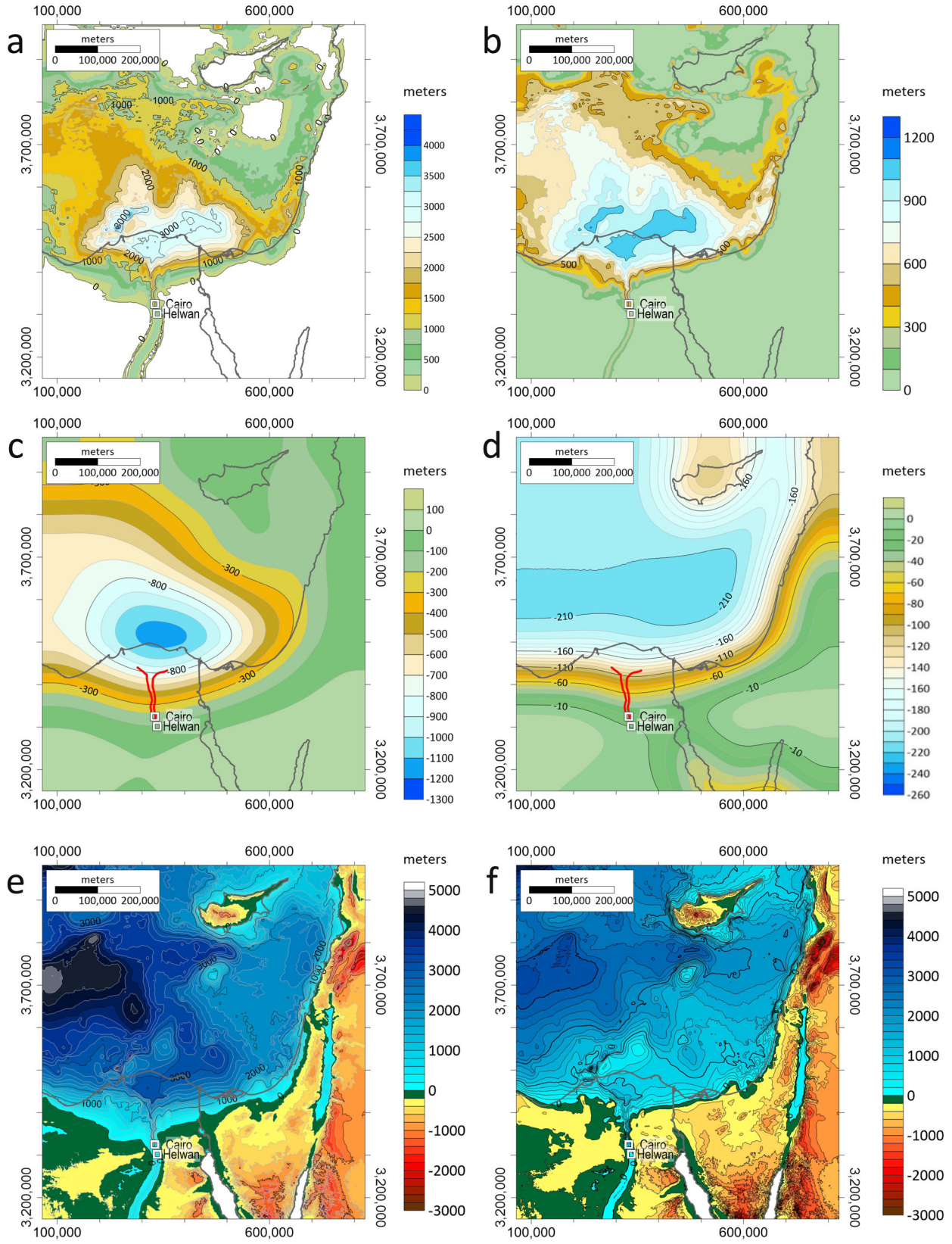

Fig. 2 Maps illustrating how the Messinian erosional surface (MES ~ base Pliocene) is restored to its original vertical position. a Thickness of rocks covering the base Pliocene surface. **b** Calculated subsidence due to compaction of pre-Pliocene sediments assuming shale lithology (for other lithologies see Supplementary Fig. S1). **c** Calculated flexural deflection due to unloading of post-Messinian rocks, using elastic thickness, Te = 30 km (for other Te values see Supplementary Fig. S2). **d** Calculated flexural deflection due to unloading of a 650-m-thick water layer (Te = 30 km, for other values of water thickness and Te see Supplementary Fig. S3). **e** Observed base Pliocene structural map[50] (modified). **f** Restored base Pliocene surface after correcting for compaction (shale) and deflection (Te = 30 km) due to sediment unloading. No correction for water unloading has been applied here.

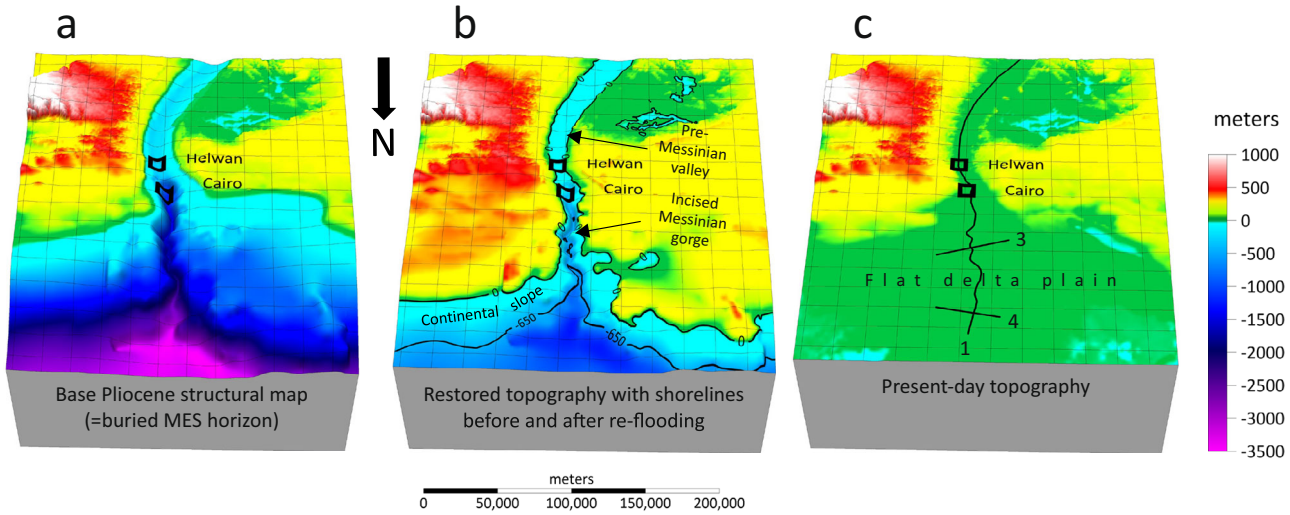

Fig. 3 3D view of the Nile delta and the buried Messinian canyon illustrating landscape evolution being restored. a Base Pliocene structural map (= MES). **b** Restored topography for the earliest Pliocene immediately after sea level recovery and prior to any Pliocene deposition (shale parameters for decompaction and Te = 30 km for deflection, same as Fig. 2 f). The isobath 650 m represents the fallen MSC shoreline. **c** Present-day topography. Black lines mark locations of cross sections (Fig. 4). Part of the area annotated as "flat delta plain" in the present topography (**c**) was a few hundred m asl in the earliest Pliocene (**b**).

observed at the far ends of the profile (Figs. 4a and 5a). This restoration is calculated for a filled Mediterranean, a short moment after it returned to "normal" (pre- and post-MSC) sea level (the absence of large glaciations at the time allows to assume Zanclean sea level close to present[26]). To restore the topography immediately before re-flooding, we unloaded a 650 m-thick water layer, generating an isostatic rebound that brings the MSC coastline to 600 mbsl (Fig. 4b) and, thus, conclude that a 600 m drawdown best explains the observations. Considering that sea level of a closed basins commonly fluctuates, we cannot rule out short episodes of lower or higher sea level. However, the observed sub-horizontal segment of the river profile indicates relative stability of the base level around 600 mbls for a duration that is long enough to produce such a profile.

Uncertainties related to decompaction and deflection. The unknown lithology and spatiotemporal distribution of the sediments buried under the Pliocene-Quaternary section, produces an uncertainty related to the parameters used for the decompaction correction. To illustrate the range of this uncertainty, we used parameters of three lithologies: sand, shale, and shaley sand (Fig. S1). Considering that at least since the Late Eocene, huge amounts of clastics started arriving to the Egyptian continental margin, which accumulated mainly shales[29,56–59], we corrected for decompaction using shale parameters and reached the conclusion of 600 m drawdown (Fig. 5b). In addition, we demonstrate that using shaly sand lithology for the pre-Pliocene sediments, the amplitude of the reconstructed drawdown may increase to 750 m (Fig. 5c).

Another source of uncertainty is related to the elastic thickness used for the deflection correction. Previous studies dealing with lithospheric strength in the studied region argued that rigidity increases along with decreasing crustal thickness[60]. Te = 45 km was used for the Levant margin[61], Te = 25 km for the Arabian plate[61], Te = 30 km for the Levant Basin, assuming that this is approximately the depth of the 350^0 isotherm[62], and Te of 10–35 km for the Levant continental margin[63].

In light of this uncertainty, here we calculated the deflection four times using Te = 20, 30, 40, and 50 km. We show that this range significantly (±400 m) influences the results in the central basin (Fig. S2), but its influence on the restored coastline is smaller than 100 m (Fig. 5b, c).

Unloading of a 650 m thick water layer causes an isostatic rebound of 210 m in the deep basin and zero inland (Fig. S3, Fig. 4b). To further show this effect we recalculate water unloading for a 500 and 750 m thick water layer, for Te = 30 amd 40 km (Fig. S3). The effect of these variations on the restored river profile are negligible (Fig. S3).

Discussion

The restored topography, during the time immediately after re-flooding and just before initial Pliocene deposition, indicates the existence of a deep-water embayment extending to the Cairo-Helwan knickzone, and a 200 m deep water body continuing farther inland (Figs. 2e and 3b). We argue that the deep embayment was excavated by Messinian incision whereas the upper valley south of the Cairo-Helwan knickzone, may have been shaped by pre-Messinian ancestors of River Nile and unaffected by the Messinian incision. This conclusion is consistent with the sedimentological data presented above indicating a transition from deep water deposits north of Cairo to shallow water and lacustrine and fluvial deposits in the Beni-Suef region and farther south along the Nile Valley; it disagrees with suggestions that the Messinian incision and subsequent marine invasion had reached Aswan.

Another indication for limited retrograde incision up to Cairo (~100 km) and not further upstream to Aswan (~1200 km) is the absence of a thick Messinian fan delta, which is expected in a case of enormous erosion along 1200 km. The Late Messinian Qawasim and Abu-Madi Formations, exceed thickness of 1000 m only in a limited (100 × 25 km) region at the mouth of the canyon[23,29,64–66]. Outside this region these formations rapidly thinn to a few 10 s or 100 s of m (<300 m) resembling distal deep water deposits[29,67,68]. Such a canyon fill with a relatively small lowsrtand fan is better reconciled with limited incision of the Messinian Nile canyon up to Cairo.

Messinian deposits of the Abu Madi and Qawasim Fm. overlying the MES offshore Egypt[23] and the MSC Stage 3 deposits overlying the salt in the Levant Basin (100–200 m thick[7,69]), indicate that the major drawdown occurred during the second

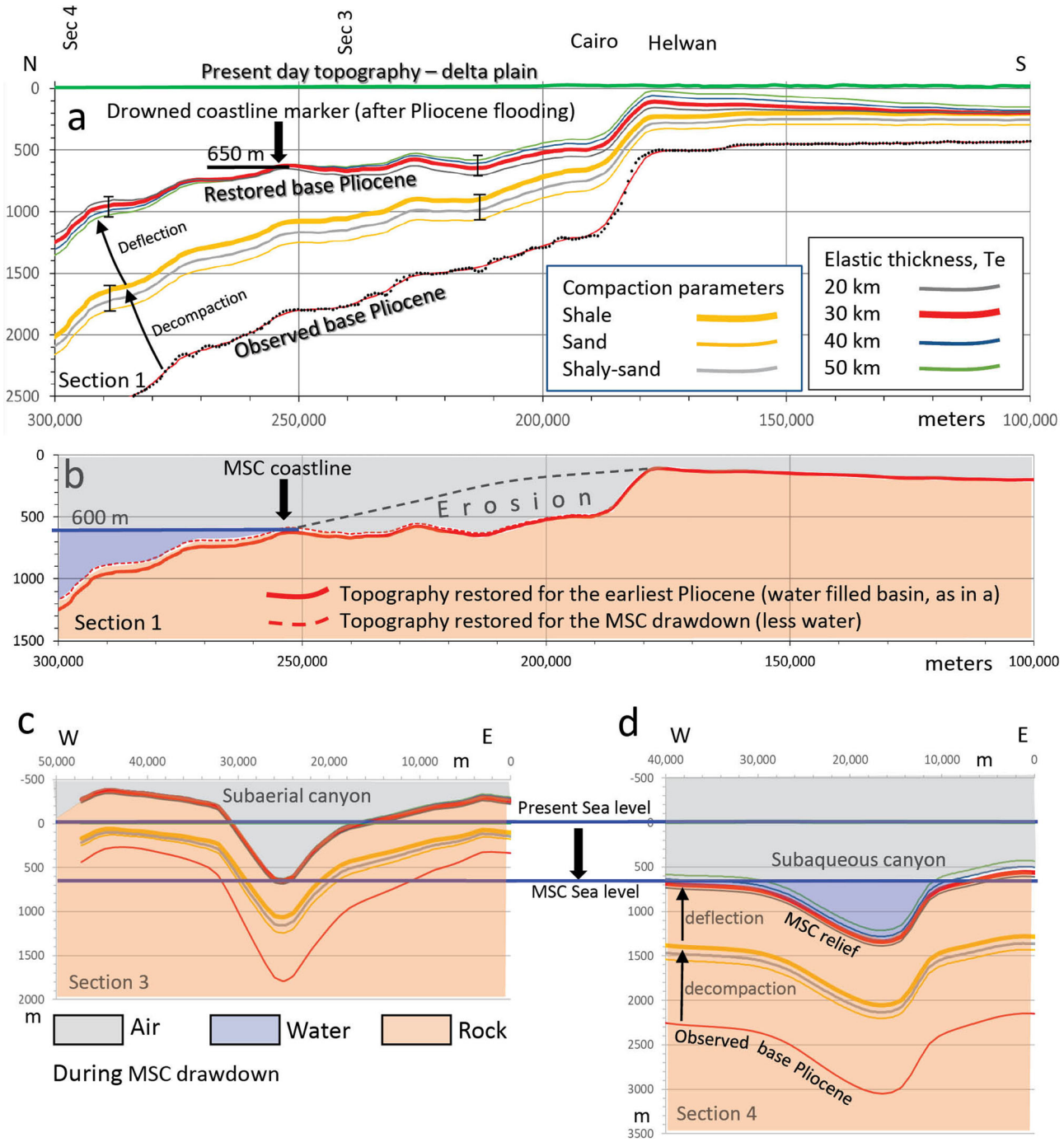

Fig. 4 Topography restoration illustrated in cross sections (location in Fig. 3c). a Along thalweg river profile illustrating the combined effect of sediment decompaction (shale parameters) and flexural deflection. Error bars represent the range of uncertainty in the decompaction (shale, sand, shaly-sand) and elastic thickness (Te = 20, 30, 40, and 50 km). **b** Interpretation of the restored river profile. The Cairo-Helwan knickzone is inferred as the southernmost location of the Messinian retrogressive incision, separating the MSC canyon gorge from the pre-MSC hanging valley. The transition from sub-horizontal to steeper gradient marks the MSC coast line 650 m below the present day sea level. **c** Restored profile across the subaerial segment of the canyon with incision down to 650 m below the pre- and post-MSC sea level. **d** Restored profile across the subaqueous part of the canyon.

stage of the MSC alongside massive salt deposition in the deep basin. However, since the thickness of the post salt Messinian deposits (MSC stage 3) are negligible in relations to the Pliocene-Quaternary section, here we assume that the top salt and the base Pliocene surfaces approximately coincide. Thus, the restored landscape at the end of Stage 2 (5.55 Ma[17]) and at the end of Stage 3 (5.33 Ma[17]) are practically the same.

The 200 m depth of the pre-Messinian upper valley south of Helwan is difficult to explain, considering that Oligocene-Miocene eustatic drawdowns only reached a few tens of meters[26]. To reconcile this discrepancy geodynamically, ~150 m regional subsidence should be invoked, as proposed from modeling of mantle-flow-sourced topography[70]; such post-Messinian tectonic correction implies reduction of the amplitude of

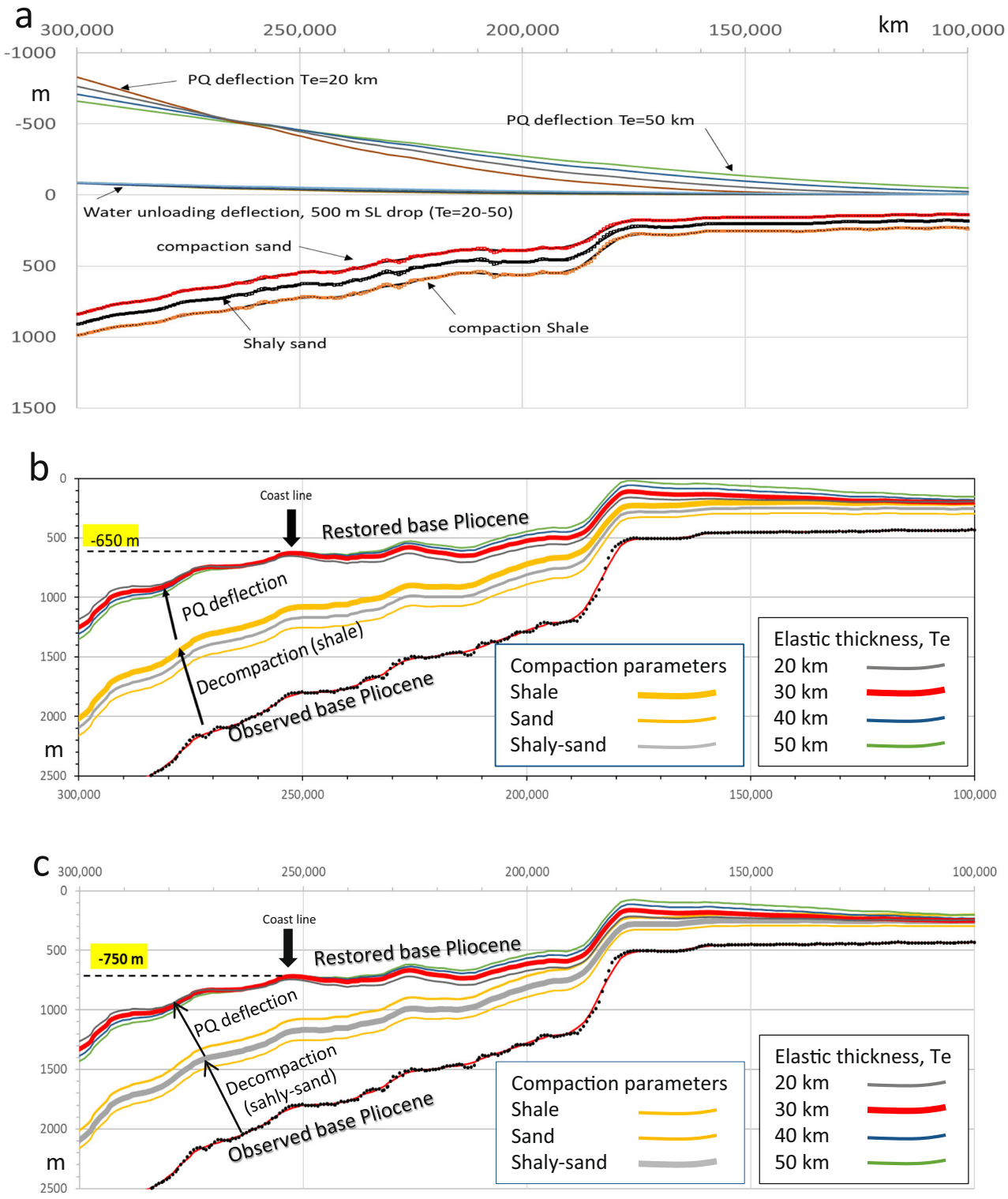

Fig. 5 Uncertainties in river profile restoration. a Calculated subsidence during burial of pre-Pliocene sediments using compaction parameters of shale, sand, and shaly-sand. Calculated deflection due to unloading of post-Messinian sediments using elastic thickness Te = 20, 30, 40, and 50 km. **b** Restoration based on the assumption that pre-Pliocene sediments are mostly shales (same as Fig. 4a). **c** Restoration based on the assumption that pre-Pliocene sediments are mostly shaly sand. The difference between **b** and **c** is 100 m in the sea level restoration (650 m versus 750 m, respectively).

drawdown from 600 m to 450 m. On the other hand, the presence of Pliocene marine rocks in the upper Nile Valley, 50 m above sea level[34], indicates that northern Egypt has not been subsiding significantly, at least since the Pliocene and, therefore, 450 m for drawdown, seems unrealistic to our opinion.

Another possibility is that the canyon depth near Helwan is not 550 mbsl[32,33], as we used for modeling, but only 200 mbsl as observed in a water well, located a few km to the south[29]. Applying 200 mbsl in the model, the restored upper valley rises to ~100 mbsl; considering post-Messinian 50 m of tectonic

subsidence, the base of the restored Miocene valley rises to 50 mbsl, which is within the range of eustatic falls. With such a tectonic correction (50 m), the inferred MSC drawdown is reduced from 600 to 550 m. It should be mentioned, however, that such details are within the uncertainties of the technique (e.g., sediment thickness, compaction, and elastic thickness) as illustrated in the Supplementary Figs. S1–S3.

Within the range of 550–750 m drawdown, we prefer the value of 600 m, which fits the assumptions of shale dominated lithology for pre-Pliocene lithology and tectonic stability of the Egyptian continental margin. ~600 m drawdown is 2–4 times smaller than previous estimations deduced from the Nile canyon[23,44,45]. We claim that previous studies underestimated the post-Messinian subsidence by ignoring the compaction of the pre-Pliocene sediments and not considering the 3D-effect of flexure. For instance, the formerly[45] estimated post-Messinian subsidence of 750–1000 m at the base of the continental slope, becomes ~2000 m when including decompaction and flexural isostasy. We further propose that base level drop and incision depth were overestimated by ignoring the uplifted canyon shoulders (*e*) and its subaqueous downstream portion (*d*) (Fig. 1b). For instance, Barber[23] measured a > 2000 m relief along the buried gorge and associated it with base-level drop. Here, we show that after isostatic unloading, the river profile reveals a flat region consistent with a steady lowered base level during the MSC at about −650 m.

The difference between our result of a 600 m drawdown and the 800–900 m drawdown inferred from the Po Plain and north Adriatic Sea[15] (same method) is within the range of uncertainty of the method. The discrepancy may therefore be related to 1) limitations of the technique (uncertainties are shown in Fig. 5 and Supplementary Figs. S1–S3); 2) The possibility of disconnected Adriatic Sea from the Eastern Mediterranean, consequently having different base levels[15], or 3) Involvement of difficult-to-correct tectonic motions in the Po Plain, located between the active Apennines and Alps. We emphasize again that, in contrast, the tectonically-stable Egyptian continental margin provide ideal conditions for restoration.

Finally, we cannot dismiss the possibility that geomorphological markers identified at various depths below the Mediterranean seabed[7,8,11], represent different and possibly shorter-lived stages of the MSC. Our analysis is based on the incision along the Messinian Nile canyon, the largest erosional feature formed during the MSC and hence we interpret it as representative for the average sea level during most of the duration of the drawdown stage.

Methods

For unloading the post-Messinian (Pliocene-Quaternary) sediments from the base Pliocene surface, we first expanded the recently compiled base Pliocene map[50] a few hundred kilometers south of Cairo. In practice this requires to reconstruct the depth of the buried canyon under the present-day Nile Valley. Outside the valley the thickness of post Messinian rocks is negligible. Based on the data presented above, we considered a linear gradient of 1/30 (1000 m over a distance of 30 km) between Cairo and Helwan and a much smaller gradient of 1/3333 (300 m per 1000 km) farther south. In this map the bottom of the canyon is 1200 m near Cairo, 550 m in Helwan[32,33], and 400 m at the southern boundary of the map (Fig. 2a).

For decompaction of underlying sediment, we used a regional sediment thickness map[71], which is >10 km deep in most of the study area. The decompaction results are insensitive to the accuracy of this map, because rocks deeper than ~5 km retain nearly negligible porosity[15,72]. The uncertainty related to a range of decompaction parameters (shale, sand, and shaly-sand) are presented in Fig. 5.

For flexural backstripping we apply an elastic thin-plate approach with a pseudo-3D (planform) flexural procedure[15,46,73]. For density of the post-Messinian sediments we use 2000 kg/m^3, consistent with seismic and well log data[71,72]. For elastic thickness we use 20, 30, 40, and 50 km and discuss the associated uncertainty in the Supplementary Fig. S2. For decompaction of underlying sediment, we used a regional sediment thickness map[74], which is >10 km deep in most of the study area. The decompaction results are insensitive to the accuracy of this map, because rocks deeper than ~5 km retain nearly negligible porosity[15,72]. The uncertainty related to a range of decompaction parameters (shale, sand, and shaly-sand) are shown in the Supplementary Fig. S1.

Data availability

The basic input for the backstripping analysis is maps compiled and modified from the literature. In particular, we used the base Pliocene structural map and the resulting Plio-Quaternary thickness map (https://doi.org/10.1130/G47031.1; http://www.geosociety.org/datarepository/2020/), which is the difference between base Pliocene and bathymetry maps. No datasets were generated during the current study.

Code availability

The code developed is named TISC and is freely available at https://github.com/danigeos/tisc.

Received: 19 July 2021; Accepted: 26 August 2022;
Published online: 20 September 2022

References

1. Hsü, K. J., Ryan, W. B. F. & Cita, M. B. Late Miocene desiccation of the Mediterranean. *Nature* **242.5395**, 240–244 (1973).
2. Ryan, W. B. F. & Cita, M. B. The nature and distribution of Messinian erosional surfaces—Indicators of a several-kilometer-deep Mediterranean in the Miocene. *Marine Geol.* **27.3-4**, 193–230 (1978).
3. Krijgsman, W. et al. Chronology, causes and progression of the Messinian salinity crisis. *Nature* **400**, 652–655 (1999).
4. Manzi, V. et al. Age refinement of the Messinian salinity crisis onset in the Mediterranean. *Terra Nova.* **25**, 315–322 (2013).
5. Ryan, W. B. F. Quantitative evaluation of the depth of the western Mediterranean before, during and after the Late Miocene salinity crisis. *Sedimentology* **23.6**, 791–813 (1976).
6. Lofi, J. et al. Erosional processes and paleo-environmental changes in the Western Gulf of Lions (SW France) during the Messinian Salinity Crisis. *Marine Geol.* **217**, 1–30 (2005).
7. Madof, A. S., Bertoni, C. & Lofi, J. Discovery of vast fluvial deposits provides evidence for drawdown during the late Miocene Messinian salinity crisis. *Geology* **47.2**, 171–174 (2019).
8. Micallef, A. et al. Evidence of the Zanclean megaflood in the eastern mediterranean basin. *Scientific Rep.* **8**, 1–8 (2018).
9. Clauzon, G. Le canyon messinien du Rhone; une preuve decive du desiccated deep-basin model(Hsue, Cita and Ryan, 1973). *Bulletin de la Société géologique de France* **7.3**, 597–610 (1982).
10. Druckman, Y., Buchbinder, B., Martinotti, G. M., Tov, R. S. & Aharon, P. The buried Afiq Canyon (eastern Mediterranean, Israel): a case study of a Tertiary submarine canyon exposed in Late Messinian times. *Marine Geol.* **123**, 167–185 (1995).
11. Bertoni, C. & Cartwright, J. A. Controls on the basinwide architecture of late Miocene (Messinian) evaporites on the Levant margin (Eastern Mediterranean). *Sediment. Geol.* **188**, 93–114 (2006).
12. Bertoni, C. & Cartwright, J. A. Major erosion at the end of the Messinian Salinity Crisis: evidence from the Levant Basin, Eastern Mediterranean. *Basin Res.* **19**, 1–18 (2007).
13. Cartwright, J. A. & Jackson, M. P. A. Initiation of gravitational collapse of an evaporite basin margin: The Messinian saline giant, Levant Basin, eastern Mediterranean. *Geological Soc. America Bull.* **120**, 399–413 (2008).
14. Urgeles, R. et al. New constraints on the Messinian sealevel drawdown from 3D seismic data of the Ebro Margin, western Mediterranean. *Basin Res.* **23**, 123–145 (2011).
15. Amadori, C. et al. Restored topography of the Po Plain-Northern Adriatic region during the Messinian base-level drop—Implications for the physiography and compartmentalization of the palaeo-Mediterranean basin. *Basin Res.* **30**, 1247–1263 (2018).
16. Ben-Moshe, L, Ben-Avraham, Z, Enzel, Y, & Schattner, U. Estimating drawdown magnitudes of the Mediterranean Sea in the Levant basin during the Lago Mare stage of the Messinian Salinity Crisis. *Marine Geol.* **427**, 106215 (2020).
17. Roveri, M. et al. The Messinian Salinity Crisis: past and future of a great challenge for marine sciences. *Marine Geol.* **352**, 25–58 (2014).
18. Roveri, M. et al. The Messinian salinity crisis: open problems and possible implications for Mediterranean petroleum systems. *Petroleum Geosci.* **22**, 283–290 (2016).
19. Schmalz, R. F. Deep-water evaporite deposition, a genetic model. *American Asso. Petroleum Geologists Bull.* **53**, 798–823 (1969).
20. Sirota, I., Enzel, Y. & Lensky, N. G. Halite focusing and amplification of salt layer thickness: From the Dead Sea to deep hypersaline basins. *Geology* **46**, 851–854 (2018).

21. Clauzon, G. The eustatic hypothesis and the pre-Pliocene cutting of the Rhône valley. In: Ryan, W. B. F., Hsü, K. J. (Eds.), Initial Reports of the Deep Sea Drilling Project, 13. U.S. Government Printing Office, Washington D.C., pp. 1251–1256, (1973).
22. Clauzon, G. Le canyon messinien du Rhone, une preuve décisive du desiccated deep-basin model (Hsü, Cita et Ryan, 1973). *Bulletin de la Societe Geologique de France* **24**, 597–610 (1982).
23. Barber, P. M. Messinian subaerial erosion of the proto-Nile Delta. *Marine Geol.* **44**, 253–272 (1981).
24. Ryan, W. B. Decoding the Mediterranean salinity crisis. *Sedimentology* **56**, 95–136 (2009).
25. Gorini, C., Montadert, L. & Rabineau, M. New imaging of the salinity crisis: Dual Messinian lowstand megasequences recorded in the deep basin of both the eastern and western Mediterranean. *Marine Petroleum Geol.* **66**, 278–294 (2015).
26. Miller, K. G. et al. The Phanerozoic record of global sea-level change. *Science* **310**, 1293–1298 (2005).
27. Chumakov, I. S. *Pliocene and Pleistocene deposits of the Nile Valley: Nubia and Upper Egypt (in Russian). Academy of Science of the USSR, Transactions of the Geological Institute* **170**, 5 (1967).
28. Chumakov, I. S. Pliocene and Pleistocene deposits of the Nile Valley in Nubia and Upper Egypt. In: Ryan, W. B. F., Hsü, K. J. (Eds.), Initial Reports of the Deep Sea Drilling Project, 13. U.S. Gov. Print. Off., Washington, DC, pp. 1242–1243 (1973).
29. Said, R., The Geological Evolution of the River Nile. Springer-Verlag, Berlin, 151 p. (1981).
30. Roveri, M., Manzi, V., Bergamasco, A. & Falcieri, F. M. Rocco Gennari, Stefano Lugli, and B. C. Schreiber. Dense shelf water cascading and Messinian canyons: a new scenario for the Mediterranean salinity crisis. *American J. Sci.* **314**, 751–784 (2014).
31. Philobbos, E. R., Essa, M. A. & Ismail, M. M. Geologic history of the Neogene Qena Lake developed during the evolution of the Nile Valley: A sedimentological, mineralogical and geochemical approach. *J. African Earth Sci.* **101**, 194–219 (2015).
32. RIGW (Research Institute for Groundwater, Egypt). Hydrogeological Map of Egypt, Scale 1:500000, Beni Suef Map Sheet (1997).
33. Awad, S. R. Groundwater hydrogeology and quality in Helwan area and its vicinities in Egypt. *Water Sci.* **33**, 10–21 (2019).
34. Sallam, E., Issawi, B., Osman, R. & Ruban, D. Deposition in a changing paleogulf: evidence from the Pliocene–Quaternary sedimentary succession of the Nile Delta, Egypt. *Arabian J. Geosci.* **11**, 558 (2018).
35. Blanckenhorn M. Handbuch der regionalen geologie, bd., vii, abt. 9, Heft 23, Agypten. Heidelberg, 244p (1921).
36. Sandford, K. S, & Arkell, W. J. Paleolithic man and the Nile-Faiyum divide (1929).
37. Little, O. H. *Recent geological work in the Faiyum and in the adjoining portion of the* Nile Valley. Inst. Français d'Archéologie Orientale (1936).
38. Hassan, M. Y., Issawi, B., & Zaghloul, E. A. Geology of the area east of Beni Suef, eastern Desert, Egypt. *Ann. Geol. Surv. Egypt*. **8**, 129–162 (1978).
39. Tateo, F., Sabbadini, R. & Morandi, N. Palygorskite and sepiolite occurrence in Pliocene lake deposits along the River Nile: Evidence of an arid climate. *J. African Earth Sci.* **31**, 633–645 (2000).
40. Mahmoud, H. H. & Tawfik, M. Z. Impact of the geologic setting on the groundwater using geoelectrical sounding in the area southwest of Sohag–Upper Egypt. *J. African Earth Sci.* **104**, 6–18 (2015).
41. Norman, S. E. & Chase, C. G. Uplift of the shores of the western Mediterranean due to Messinian desiccation and flexural isostasy. *Nature* **322**, 450–451 (1986).
42. Gargani, J. Modelling of the erosion in the Rhone valley during the Messinian crisis (France). *Quaternary Int.* **121**, 13–22 (2004).
43. Govers, R., Meijer, P. & Krijgsman, W. Regional isostatic response to Messinian Salinity Crisis events. *Tectonophysics* **463**, 109–129 (2009).
44. Gargani, J., Rigollet, C. & Scarselli, S. Isostatic response and geomorphological evolution of the Nile valley during the Messinian salinity crisis. *Bulletin de la Société Géologique de France* **181**, 19–26 (2010).
45. Gargani, J., & Rigollet, C. Mediterranean Sea level variations during the Messinian salinity crisis. *Geophys. Res. Lett.* **34**, https://doi.org/10.1029/2007GL029885 (2007).
46. Heida, Hanneke et al. Flexural-isostatic reconstruction of the Western Mediterranean during the Messinian Salinity Crisis: Implications for water level and basin connectivity. *Basin Research* **34**, 50–80 (2022). no. 1.
47. Robertson, A. H. F., & Dixon, J. E. Introduction: aspects of the geological evolution of the Eastern Mediterranean. Geological Society, London, Special Publications, 17, 1-74. (1984).
48. Faccenna, C. et al. Mantle dynamics in the Mediterranean. *Reviews of Geophysics* **52**, 283–332 (2014).
49. Faccenna, C., & Becker, T. W. Topographic expressions of mantle dynamics in the Mediterranean. *Earth-Sci. Rev.* **103327** (2020).
50. Zucker, E., Gvirtzman, Z., Steinberg, J. & Enzel, Y. Salt tectonics in the Eastern Mediterranean Sea: Where a giant delta meets a salt giant. *Geology* **48**, 134–138 (2020).
51. Ghielmi, M. et al. Sedimentary and tectonic evolution in the eastern Po-Plain and northern Adriatic Sea area from Messinian to Middle Pleistocene (Italy). *Rendiconti Lincei* **21**, 131–166 (2010).
52. Ghielmi, M., Minervini, M., Nini, C., Rogledi, S. & Rossi, M. Late Miocene–Middle Pleistocene sequences in the Po Plain–Northern Adriatic Sea (Italy): the stratigraphic record of modification phases affecting a complex foreland basin. *Marine Petroleum Geol.* **42**, 50–81 (2013).
53. Liu, J. T. et al. From the highest to the deepest: The Gaoping River–Gaoping Submarine Canyon dispersal system. *Earth-Sci. Rev.* **153**, 274–300 (2016).
54. Amblas, D., Canals, M. & Gerber, T. P. The long-term evolution of submarine canyons: insights from the NW Mediterranean. *CIESM Monogr.* **47**, 171–181 (2015).
55. Haviv, I. et al. Evolution of vertical knickpoints (waterfalls) with resistant caprock: Insights from numerical modeling. *J. Geophys. Res.: Earth Surf.* **115**, pp. 1–22 (2010).
56. Salem, Rafik Evolution of Eocene-Miocene sedimentation patterns in parts of northern Egypt. *AAPG Bulletin* **60**, 34–64 (1976).
57. Steinberg, Josh, Gvirtzman, Zohar, Folkman, Yehoshua & Garfunkel, Zvi Origin and nature of the rapid late Tertiary filling of the Levant Basin. *Geology* **39**, 355–358 (2011).
58. Macgregor, Duncan S. The development of the Nile drainage system: integration of onshore and offshore evidence. (2012): 417–431.
59. Bar, Oded, Zilberman, Ezra, Feinstein, Shimon, Calvo, Ran & Gvirtzman, Zohar. The uplift history of the Arabian Plateau as inferred from geomorphologic analysis of its northwestern edge. *Tectonophysics* **671**, 9–23 (2016).
60. Steckler, M. S. & U. ten Brink. Lithospheric strength variations as a control on new plate boundaries: Examples from the northern Red Sea region: *Earth Planetary Lett.* **79**, 120-132 (1986).
61. Ten Brink, U. S. Schoenberg, N., Kovach, R. L. & Ben-Avraham, Z. Uplift and a possible Moho offset across the Dead Sea transform. *Tectonophysics* **180**, 71–85 (1990).
62. Segev, A., Michael R., Vladimir L., Avraham H., Gidon T., Vladimir G., & Zvi Ben A. The structure, isostasy and gravity field of the Levant continental margin and the southeast Mediterranean area. *Tectonophysics* **425**, 1–4 (2006): 137–157.
63. Steinberg, J., Gvirtzman, Z. & Garfunkel, Z. Flexural response of a continental margin to sedimentary loading and lithospheric rupturing: The mountain ridge between the Levant Basin and the Dead Sea Transform. *Tectonics* **33**, 166–186 (2014).
64. Rizzini, Antonio, Vezzani, Franco, Cococcetta, Vincenzo & Milad, George Stratigraphy and sedimentation of a Neogene—Quaternary section in the Nile Delta area (ARE). *Marine Geol.* **27**, 327–348 (1978).
65. Pigott, JohnD. & Abdel-Fattah, MohamedI. Seismic stratigraphy of the Messinian Nile Delta coastal plain: Recognition of the fluvial Regressive Systems Tract and its potential for hydrocarbon exploration. *J. African Earth Sci.* **95**, 9–21 (2014).
66. Leila, Mahmoud & Moscariello, Andrea Seismic stratigraphy and sedimentary facies analysis of the pre-and syn-Messinain salinity crisis sequences, onshore Nile Delta, Egypt: implications for reservoir quality prediction. *Marine Petroleum Geol.* **101**, 303–321 (2019).
67. Ahmed, AbdelAal et al. Tectonic evolution of the eastern Mediterranean Basin and its significance for the hydrocarbon prospectivity of the Nile Delta deepwater area. *GeoArabia* **6**, no. 3 363–384 (2001).
68. Kellner, A., Brink, G. J. & El, H. Khawaga. Depositional history of the western Nile Delta, Egypt: Late Rupelian to Pleistocene. *AAPG Bull.* **102**, 1841–1865 (2018).
69. Gvirtzman, Z. et al. Intra-Messinian truncation surface in the Levant Basin explained by subaqueous dissolution. *Geology* **45**, 915–918 (2017).
70. Faccenna, C. et al. Role of dynamic topography in sustaining the Nile River over 30 million years. *Nat. Geosci.* **12**, 1012–1017 (2019).
71. Loncke, L., Gaullier, V., Mascle, J., Vendeville, B. & Camera, L. The Nile deep-sea fan: an example of interacting sedimentation, salt tectonics, and inherited subsalt paleotopographic features. *Marine and Petroleum Geology* **23**, 297–315 (2006).
72. Sagy, Y., Gvirtzman, Z., Reshef, M. & Makovsky, Y. The enigma of the Jonah high in the middle of the Levant basin and its significance to the history of rifting. *Tectonophysics* **665**, 186–198 (2015).
73. Garcia-Castellanos, D., Vergés, J., Gaspar-Escribano, J., & Cloetingh, S. Interplay between tectonics, climate, and fluvial transport during the Cenozoic evolution of the Ebro Basin (NE Iberia). *J. Geophysical Res.: Solid Earth* **108**, (2003).
74. Laske, G., Masters, G., Ma, Z. & Pasyanos, M. Update on CRUST1. 0-A 1-degree Global Model of Earth's Crust. EGU General Assembly Conference Abstracts, p. 2658 (2013).

Acknowledgements
The article was supported by COST Action "Uncovering the Mediterranean salt giant" (MEDSALT), funded by the European Cooperation in Science and Technology. It was also supported by the SALTGIANT program, a European project funded by the European Union's Horizon 2020 research and innovation program under the Marie Sklodowska Curie grant agreement number 765256. We appreciate the thorough review and constructive comments by Joe Cartwright and another anonymous reviewer, that significantly improved the manuscript.

Author contributions
Z.G. initiated the study, guided E.Z., prepared all grids for simulations, and led the writing; H.H. ran the 3D backstripping calculations; O.B. provided the geological data about the Nile Valley and set the base for the geomorphological analysis; E.Z. compiled the Base Pliocene map from numerous sources. D.G-C. developed the code for backstripping, guided H.H., and participated in the flexural and geomorphological analysis. Y.E. contributed to the geomorphological analysis and writing and guided E.Z. All authors participated in discussions and writing.

Competing interests
The authors declare no competing interests.

Additional information
Supplementary information The online version contains supplementary material available at https://doi.org/10.1038/s43247-022-00540-4.

Correspondence and requests for materials should be addressed to Zohar Gvirtzman.

Peer review information *Communications Earth & Environment* thanks Joe Cartwright and the other, anonymous, reviewer(s) for their contribution to the peer review of this work. Primary Handling Editor: Joe Aslin.